Electronic Supplementary Material (ESI) for Chemical Communications

A modular system for regeneration of NAD cofactors using graphite particles modified with hydrogenase and diaphorase moieties

Holly A. Reeve, Lars Lauterbach, Philip A. Ash, Oliver Lenz and Kylie A. Vincent

Electronic Supplementary Information

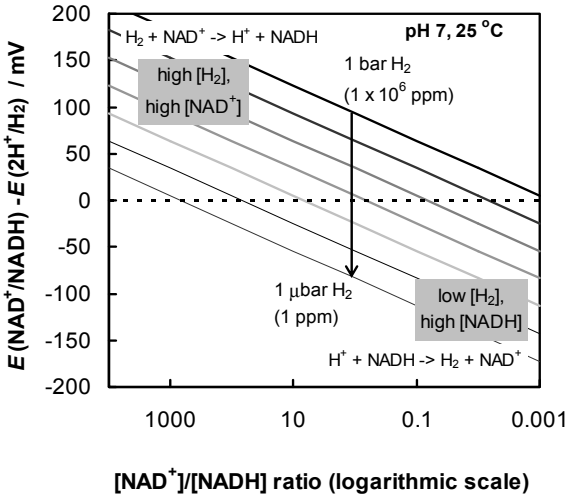

Fig. S1. Representation of the thermodynamic driving force for reduction of NAD^+ by H_2 according to H_2 partial pressure and ratio of $[NAD^+]$: [NADH]. Reduction of NAD^+ by H_2 is favoured in regions of the plot where $E(NAD^+/NADH) - E(2H^+/H_2)$ is positive, while the oxidation of NADH by H^+ is favoured in regions where $E(NAD^+/NADH) - E(2H^+/H_2)$ is negative.

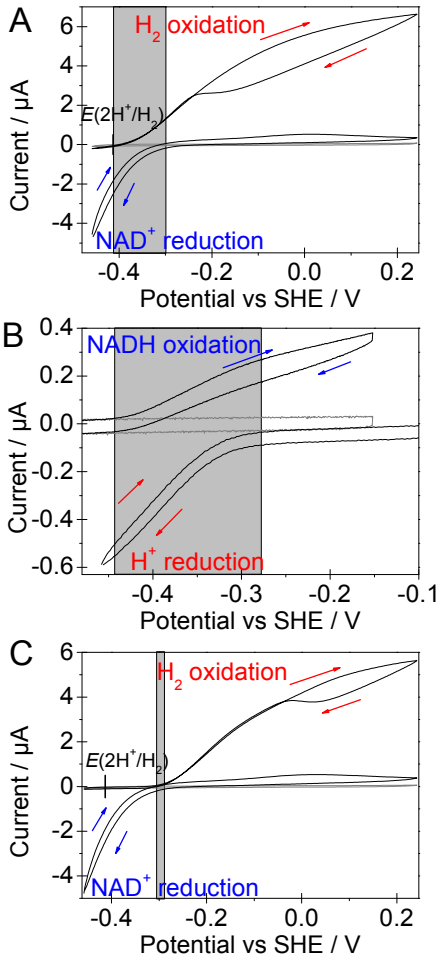

Fig. S2. Cyclic voltammograms (CVs) for different enzymes immobilised on a pyrolytic graphite rotating disk electrode. Pairs of catalytic reactions should be thermodynamically favourable when the enzymes are coupled on graphite particles in cases where oxidation of the first substrate occurs at a more negative potential than reduction of the second substrate. (A) CV showing oxidation of H_2 by *Escherichia coli* Hydrogenase 2 overlaid on CV showing NAD^+ reduction by *Ralstonia eutropha* HoxFU (under these conditions NAD^+ reduction by H_2 should be favourable); (B) CV showing reduction of H^+ by *E. coli* Hydrogenase 2 overlaid on CV showing NAD^+ reduction by *R. eutropha* HoxFU (under these conditions, NADH oxidation by H^+ should be favourable); (C) CV showing oxidation of H_2 by *R. eutropha* MBH overlaid on CV showing NAD^+ reduction by *R. eutropha* HoxFU (demonstrating that the overpotential exhibited by MBH for H_2 oxidation diminishes the window of potentials in which NAD^+ reduction by H_2 is favourable with this catalyst pair). In each panel, the shaded area represents the potential window in which the coupled catalysis should be favourable.

All were scans performed in a single compartment cell in 50 mM potassium phosphate buffer (pH 7) at a scan rate of 10 mV/s, and at an electrode rotation rate of 2000 rpm which is sufficiently fast that catalysis by the enzyme moieties is not limited by mass transport of substrate or product. Hydrogenase scans in panels A and C were recorded in H_2 saturated buffer (H_2: Air Products, Premier Plus); the hydrogenase scan in panel B was recorded in N_2 saturated buffer (N_2: BOC). The HoxFU scan in panels A and C was recorded in 1 mM NAD^+ solution, and the HoxFU scan in panel B was recorded in 1 mM NADH solution. In each panel, a scan at an unmodified electrode (grey) recorded at the same NAD^+ or NADH concentration confirms that the graphite electrode does not react directly with NAD^+ or NADH over the potential range of interest.

Electrochemical experiments were controlled by an Autolab potentiostat (EcoChemie 128N) and performed in an

anaerobic glove box (mBraun, O_2 < 0.1 ppm). The rotating disc electrode (RDE) was constructed from pyrolytic graphite 'edge' (Momentive Performance Materials) of planar surface area 0.03 cm^2 encased in epoxy resin, and was connected to an EG&G electrode rotator model 636. For each scan the electrode was abraded with sand paper (P800 grade, Norton Abrasives), sonicated for 10 s in milliQ purified water and rinsed before application of an enzyme film. Enzyme films were prepared by pipetting enzyme (0.5 µL) onto the electrode tip and allowing it to adsorb over ~20 seconds. The electrode was then placed into buffered electrolyte (potassium phosphate buffer, 50 mM, pH 7, prepared by titration of K_2HPO_4 and KH_2PO_4 (BDH, in milliQ water) to the required pH. Electrolyte contained substrate as specified. The reference electrode was a saturated calomel electrode (SCE, BAS) and the counter electrode was Pt wire. Potentials were converted to units of V *vs* SHE using $E(\mathrm{SHE}) = E(\mathrm{SCE}) + 0.242\,\mathrm{V}$ at 25 °C.

From the cyclic voltammogram for NAD^+ reduction shown in Fig S2A, at -0.4 V vs SHE (the lower limit at which NAD^+ reduction by H_2 is favourable under these conditions) the electrocatalytic current is 2 µA (current density 66 µA cm^{-2}). This compares favourably with a current density of 16 µA cm^{-2} reported at this potential on the first voltammetric cycle for a graphite electrode modified with a subcomplex of respiratory Complex I; furthermore the activity of the Complex I moiety was shown to rapidly switch off close to -0.4 V.[S1] Many non-enzymatic electrodes exhibit overpotentials for NAD^+ reduction that would preclude coupling to the H^+/H_2 couple;[S2] a notable exception is poly(Neutral Red) modified glassy carbon which exhibits reduction of NAD^+ to enzymatically-active NADH with a current density of at least 1 µA cm^{-2} under similar conditions.[S3]

From the cyclic voltammogram for NADH oxidation (Fig S2B), at -0.28 V (the upper limit at which NADH oxidation by H^+ is favourable under these conditions) the electrocatalytic current is 0.2 µA (current density 6.6 µA cm^{-2}). For comparison, a current density of ca 15 µA cm^{-2} was reported at this potential for the Complex I subcomplex on a graphite electrode on the first voltammetric cycle.[S1] Data on electrocatalytic NADH oxidation for a range of other electrode systems has been reported at potentials more positive than +0.2 V vs SHE reflecting the substantial overpotential requirement for this reaction at most electrodes;[S4] coupling of NADH to H^+ reduction is not feasible at such high potentials.

For HoxFU and the hydrogenases utilised in this study, we were unable to detect non-catalytic signals in electrochemical experiments carried out in the absence of substrate, and thus we could not reliably determine the electroactive coverage on an electrode. This suggests that the coverage is below 3 pmol cm^{-2}, a coverage at which non-catalytic signals are just visible for the hydrogenase from *Allochromatium vinosum*.[S5]

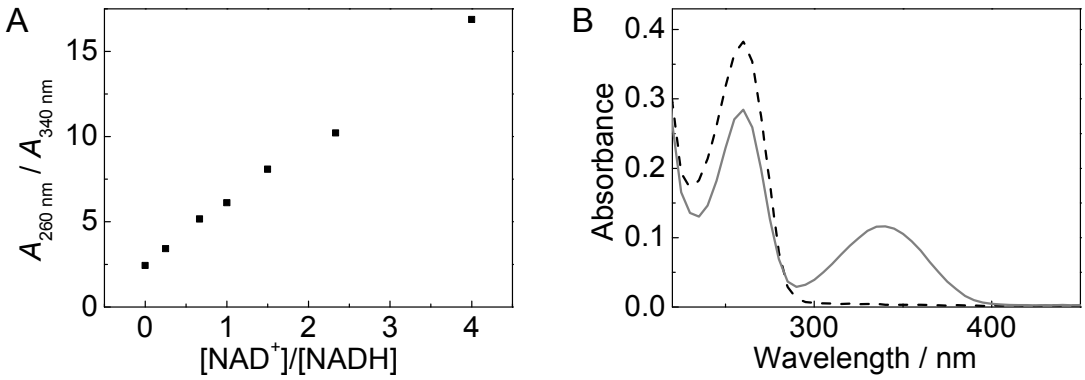

Fig. S3. Procedure for determination of the concentration ratio of NAD^+ to NADH in solution from UV absorbance (*A*) values. (A) Plot of $A_{260\ nm}/A_{340\ nm}$ vs [NAD^+]/[NADH] measured for solutions of known cofactor ratio. (B) UV spectra of NAD^+ (black) and NADH (grey).

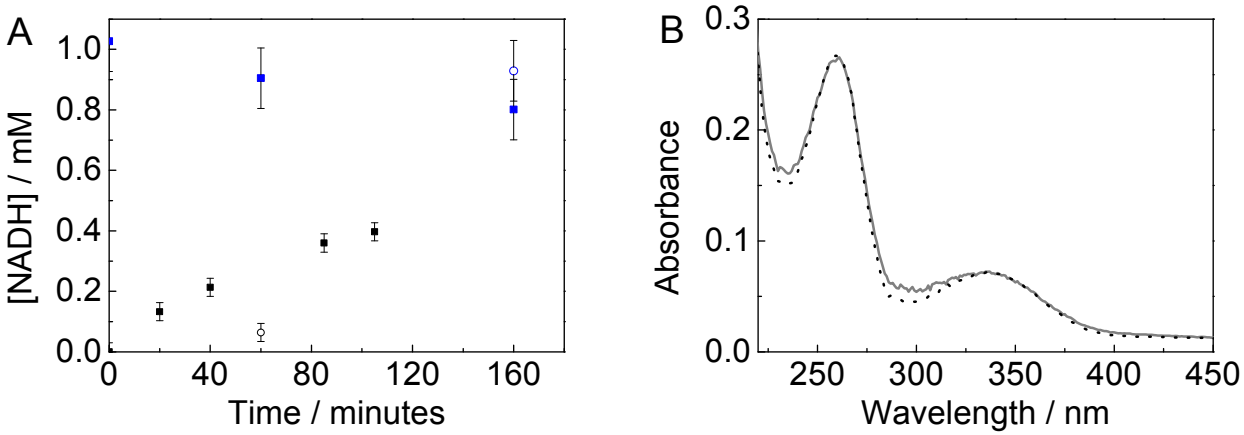

Fig. S4. Cofactor regeneration and control experiments for generation of NAD^+ from NADH and generation of NADH from NAD^+.

(A) Blue points show a time series for NAD^+ generation particles operated in 1 mM NADH under N_2 (■, reproduced from Fig. 2A) and a control experiment (○) in which the same particles were operated in 1 mM NADH under H_2. Dihydrogen is an inhibitor of H^+ reduction by [NiFe]-hydrogenases and minimises the driving force for NADH oxidation by H^+; NAD^+ production at 160 minutes was <15% of the level in the experiment under N_2. Black points show NADH generation particles operated in 1 mM NAD^+ under H_2 (■) and a control experiment (○) in which the same particles were operated in 1 mM NADH under N_2. No NADH was detected at 60 minutes for the particles operated under N_2. For this experiment *ca* 3.2 μg of *R. eutropha* HoxFU and *ca* 0.5 μg of *E. coli* Hyd-2 were mixed, and to this mixture was added *ca* 2 mg of sonicated particles in potassium phosphate buffer, pH 7.0. For each cofactor regeneration test, *ca* 0.4 mg of enzyme-modified particles were used.

(B) UV spectra recorded at 90 minutes after commencing an NADH generation reaction in 1.5 mM NAD^+ under H_2. The grey spectrum shows NADH produced on the first use of the particles; the black dashed spectrum shows NADH produced on the third cycle. Between each cycle, particles were retrieved by centrifugation and washed, and then fresh NAD^+ was introduced and the solution was re-saturated with H_2.

Error bars on NAD^+ and NADH concentrations shown in Figure 2 of the manuscript and ESI Figure S4(A) and ESI Figure S5(B) were calculated from $A_{260\,nm}/A_{340\,nm}$ data measured in triplicate for samples of known [NAD^+]/[NADH].

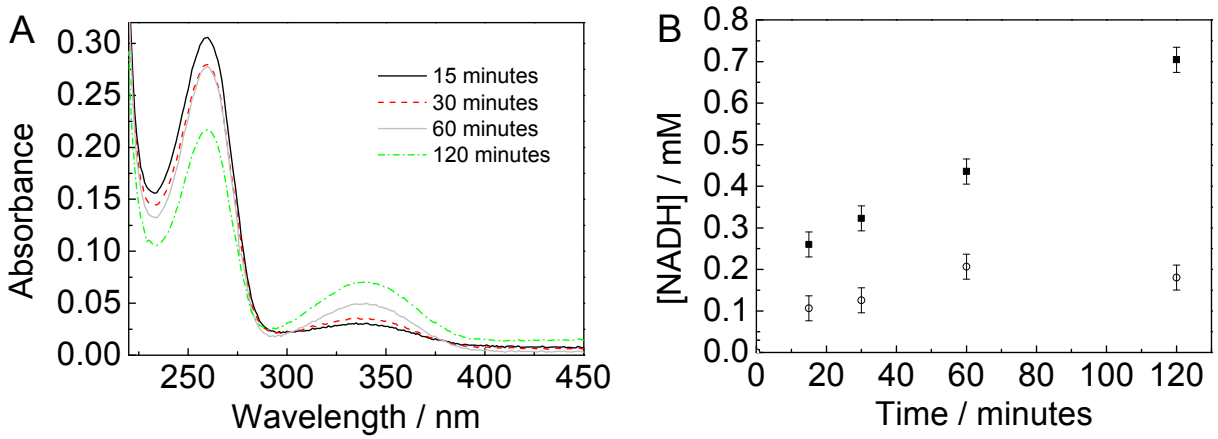

Fig. S5. Cofactor generation by platinised PG particles modified with HoxFU. (A) UV spectra showing conversion of NAD^+ to NADH by platinised particles modified with HoxFU; 88% conversion is observed at 120 minutes. (B) Time series for NADH production by particles modified with HoxFU (■, calculated from data in A) and without HoxFU (○) operating in H_2-saturated solution containing 0.8 mM NAD^+.

Platinised particles were prepared by electrochemically cycling a rod of PG (between -0.508 and 0.492 V vs SHE) in buffered (pH 7.0) hexachloroplatinate solution (10 mM) and then gently sanding particles from the surface before adding HoxFU (1.3 μg).

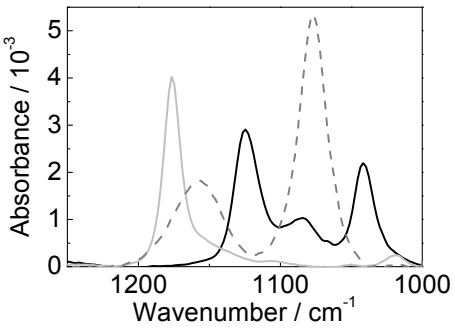

Fig. S6. Reference spectra of pyruvate, lactate and potassium phosphate buffer. ATR-IR spectra of 50 mM pyruvate (grey), 39.5 mM lactate (black) and 50 mM phosphate (dashed) in the spectral region 1000 – 1250 cm^{-1}. Pyruvate and lactate spectra were recorded at pH 6.2 in the presence of 10 mM potassium phosphate buffer, and are displayed as difference spectra after subtraction of a buffer reference (a water reference has been subtracted from the phosphate spectrum). In the lactate spectrum, the peak at 1045 cm^{-1} is assigned to the stretching vibration of the C-CH_3 bond, the weak absorbance at 1085 cm^{-1} is assigned to the alcoholic C-O stretch and the peak at 1125 cm^{-1} is due to a combination of a CH_3 bending mode with the alcoholic C-O stretching vibration.[S6] The band at 1175 cm^{-1} in the spectrum of pyruvate is a combination of C-C and C-O stretching modes due to the presence of a *gem*-diol form of the pyruvate anion in aqueous solution.[S7]

ATR-IR at a diamond ATR prism is an established method for detection of low levels of alcohols in water.[S8]

References

S1. C. D. Barker, T. Reda, J. Hirst, *Biochemistry*, 2007, **46**, 3454-3464.

S2. H.-K. Song, S.H. Lee, K. Won, J.H. Park, J.K. Kim, H. Lee, S.-J. Moon, D.K. Kim, C.B. Park, *Angew. Chem. Int. Ed.*, 2008, **47**, 1749-1752;

S3. A. A. Karyakin, Y. N. Ivanova, E. E. Karyakina, *Electrochem. Commun.*, 2003, **5**, 677–680.

S4. I. Katakis, E. Domínguez, *Mikrochim. Acta*, 1997, **126**, 11-32; L. Gorton, E. Domínguez, *Rev. Mol. Biotech.*, 2002, **82**, 371-392; R. Antiochia, L. Gorton, *Biosens. Bioelectron.*, 2007, **22**, 2611-2617.

S5. H. R. Pershad, J. L. C. Duff, H. A. Heering, E. C. Duin, S. P. J. Albracht and F. A. Armstrong, *Biochemistry*, 1999, **38**, 8992-8999.

S6. G. Cassanas, M. Morssli, E. Fabrègue, L Bardet, *J. Raman Spectroscopy*, 1991, **22**, 409-413.

S7. K. Hanai, A. Kuwae, Y. Sugawa, K.-K. Kunimoto, S. Madea, *J. Mol. Structure*, 2007, **837**, 101-106.

S8. Agilent Technologies Application Note “Quantitative analysis using ATR-FTIR Spectroscopy” March 2011 (www.agilent.com/chem).